J. Iron Steel Res. Int. (2020) 27:248–258
https://doi.org/10.1007/s42243-019-00355-2

ORIGINAL PAPER

Thermal performance evaluation of subcritical organic Rankine cycle for waste heat recovery from sinter annular cooler

Jun-sheng Feng[1] · Guang-tao Gao[2] · Yousef N. Dabwan[2] · Gang Pei[2] · Hui Dong[3]

Received: 25 November 2018 / Revised: 12 March 2019 / Accepted: 19 March 2019 / Published online: 3 January 2020

Abstract
The sinter cooling flue gas expelled from the end of an annular cooler was taken as the heat source of an organic Rankine cycle (ORC) system, and R123, R245fa, R600, R601 and R601a were selected as the working fluids of the ORC system. The effects of evaporation temperature and superheat degree of working fluid, as well as the pinch point temperature difference in the evaporator on the system thermal performance, were analyzed in detail. The results show that the system net output power and exergy efficiency for different working fluids first increase and then decrease with an increase in the evaporation temperature and decrease with an increase in the superheat degree and pinch point temperature difference. The change in pinch point temperature difference has no effect on the system thermal efficiency. For a given operational condition, the system thermal efficiency and exergy efficiency of R123 are the maximum, while the system total irreversible loss of R245fa is the maximum. When the evaporation temperature is greater than 110 °C, the system net output power of R600 is the maximum. The ORC system could obtain the maximum net output power and exergy efficiency through the adjustment of evaporation temperature of working fluid.

Keywords Sinter · Waste heat recovery · Organic Rankine cycle · Fluid selection · Performance evaluation

1 Introduction

The efficient recovery and utilization of waste heat resources in the sintering process is one of the main ways to reduce the energy consumption of sintering process and iron-making process in the iron and steel industry [1–3]. In the actual sintering process, the sinter waste heat is mainly recycled through an annular cooler, and the quantity of sinter waste heat is about 70% of the total waste heat quantity of sintering process [4]. Due to the structure setting of the annular cooler, the outlet temperature of sinter cooling flue gas gradually decreases along the operating direction of the annular cooler. For the current sinter waste heat recovery, the annular cooler mainly recycles the waste heat resource of medium–high-temperature sinter cooling flue gas with the outlet temperature above 250 °C, and the low-grade cooling flue gas with the outlet temperature below 200 °C is emitted directly into the atmosphere, which results in about 35% of the sinter waste heat quantity wasted [5]. Therefore, the efficient recovery of low-grade sinter cooling flue gas waste heat resource is of great significance to improve the recovery and utilization rate of sinter waste heat and reduce the energy consumption of sintering process.

Because the organic Rankine cycle (ORC) technology has many advantages, such as simple structure, convenient operation and high thermal efficiency, ORC has been a worldwide accepted technology of power generation by utilizing the low-grade waste heat resources compared with other dynamic energy conversion systems. Aiming at the research of low-temperature waste heat ORC technology, scholars have done a lot of work for the selection of cycle working fluid. Chen et al. [6] presented a review of the selection criteria of potential working fluids and analyzed the influence of different working fluid properties on cycle performance. Han et al. [7] selected fourteen types of working fluids by the thermodynamic and economic properties and used MATLAB simulation to obtain the optimal working

✉ Gang Pei
Peigang@ustc.edu.cn

[1] School of Environment and Energy Engineering, Anhui Jianzhu University, Hefei 230026, Anhui, China

[2] School of Engineering and Science, University of Science and Technology of China, Hefei 230026, Anhui, China

[3] School of Metallurgy, Northeastern University, Shenyang 110819, Liaoning, China

fluid. They found that the cyclohexane was an ideal working fluid with higher thermal efficiency and appropriate pressure ratio. Li et al. [8] studied the influences of different organic working fluids on the efficiency of a subcritical ORC power generation system. They found that the R245fa is better than other working fluids and the R601a working fluid can be used for the high-temperature heat source. Wang et al. [9] selected nine different pure organic working fluids according to their physical and chemical properties and analyzed the performance of different working fluids operating in specific regions. Long et al. [10] conducted an optimal analysis to illuminate the impact of working fluids on internal and external exergy efficiencies of an ORC system and concluded that the selection of working fluids depends greatly on optimal evaporation temperature. Saloux et al. [11] proposed a methodology for selecting the most appropriate ORC fluid, and the selection of the working fluid methodology is then applied to several situations of low-temperature ORCs.

Except for the selection of ORC working fluid, the thermodynamic analysis and parameter optimization of the ORC system were also widely studied by some researchers. Kaşka [12] illustrated the variations of energy and exergy efficiencies of an ORC system with evaporator/condenser pressures, superheating and sub-cooling. Javanshir et al. [13] investigated the thermodynamic performance of the regenerative ORC over a range of operating conditions for fourteen dry working fluids and concluded that adding regeneration to the cycle did not change the specific network output. Xie et al. [14] experimentally studied the effect of cooling water temperature on ORC performance by using R123 working fluid to generate power from low-grade waste heat. Fan et al. [15] built a discretized model of the evaporator with constant heat exchange area to analyze the effects of condensation temperature, evaporation temperature and mass flow rate of working fluid on the ORC performances. Pang et al. [16] experimentally compared the performance of an ORC system by using R245fa, R123 and their mixtures to generate maximum net power on simulated low-temperature industrial waste heat. Li et al. [17] experimentally investigated the performance of a small-scale ORC system using the low-grade heat sources to generate electric power and examined the effects of heat source temperature and working fluid pump speed on system performance. Roy et al. [18, 19] conducted the parameter optimization and performance analysis for a low-temperature flue gas waste heat ORC system and concluded that using R123 as working fluid could convert the low-temperature waste heat into the useful work better. Cignitti et al. [20] designed an organic Rankine cycle process and its pure working fluid simultaneously for waste heat recovery of the exhaust gas from a marine diesel engine. Sanchez et al. [21] investigated the use of binary zeotropic mixtures as working fluids applied to organic Rankine cycles, used the genetic algorithm to identify the ideal mixtures that maximized the net power and exergy efficiency and minimized the global conductance of heat exchanger for a given temperature of heat source. Chen et al. [22] optimized the evaporator heat transfer surface area and mass flow rate of working fluid to obtain the maximum power output and thermal efficiency of subcritical simple irreversible organic Rankine cycle and investigated the influences of the internal irreversibilities on the optimal performances.

To sum up, the application of ORC technology in the low-grade waste heat field has obtained a lot of research results. As known from the above research results, the physical parameters and temperature of low-temperature heat source fluid have a great influence on the selection of ORC working fluid and system performance, and thus, part of research results of low-temperature waste heat ORC have certain limitations. At present, the research on the ORC system of sinter cooling flue gas waste heat mainly focuses on the feasibility analysis of the thermal system [23, 24], and there are few researches for the influences of thermodynamic parameters on the ORC system performance. Therefore, the low-grade cooling flue gas with the outlet temperature below 200 °C at the end of a sinter annular cooler is used as the heat source fluid of the ORC system in the present work. Firstly, the suitable working fluids of the ORC system are selected according to the thermal physical property, environmental protection and safety of working fluid, as well as the system economy and temperature range of heat source fluid. And then, based on the basic ORC system model, the influences of evaporation temperature and superheat degree of working fluid, as well as the pinch point temperature difference in the evaporator on the thermal performance of the ORC system, are analyzed. The research results of this work will lay an important theoretical foundation for the subsequent parameter optimization of an ORC system for waste heat recovery of sinter cooling flue gas.

2 Selection of ORC working fluid

The reasonable selection of organic working fluid has an important influence on the cycle efficiency, net output power and total irreversible loss of an ORC system. The thermal cycling characteristics, environmental protection and security of working fluid are generally considered for the primary selection of working fluid, and the specific requirements are as follows [25–27].

1. The saturation pressure corresponding to the highest temperature of working fluid should not be too high; otherwise, additional cost of equipment under pressure would be added. In addition, the minimum saturation pressure should not be too low, and it is better to main-

tain positive pressure to prevent the infiltration of external air to affect the system performance.

2. In order to avoid the phase change of working fluid during the expansion process in the expander to affect the output power of the expander, according to the slope of saturation vapor curve of working fluid in the temperature–entropy (T–s) diagram, the dry fluid ($\mathrm{d}T/\mathrm{d}s > 0$) and isentropic fluid ($\mathrm{d}T/\mathrm{d}s \to \pm\infty$) are usually selected as the working fluid of an ORC system.
3. The ozone depletion potential (ODP) and the global warming potential (GWP) are two important environmental evaluation indexes to select the organic working fluid. Based on the relevant regulations in the Montreal Protocol, the working fluid with ODP greater than 0.05 and GWP greater than ten thousand would not be considered in the present work. In addition, the working fluid with non-toxic, non-flammable, non-explosive and non-corrosive features, as well as low price, would be with selected priority.

Based on the above selection requirements of working fluid, considering the temperature range of sinter cooling flue gas at the end of a sinter annular cooler [28], R123, R245fa, R600, R601 and R601a are selected as the working fluids of an ORC system for waste heat recovery of sinter cooling flue gas. The temperature–entropy curves of selected working fluids are shown in Fig. 1, and R123 and R245fa are the isentropic fluids, while R600, R601 and R601a are the dry fluids. In addition, these five types of working fluids are also the environment-friendly organic working fluids, and the detailed characteristic parameters of five types of working fluids are listed in Table 1 [7].

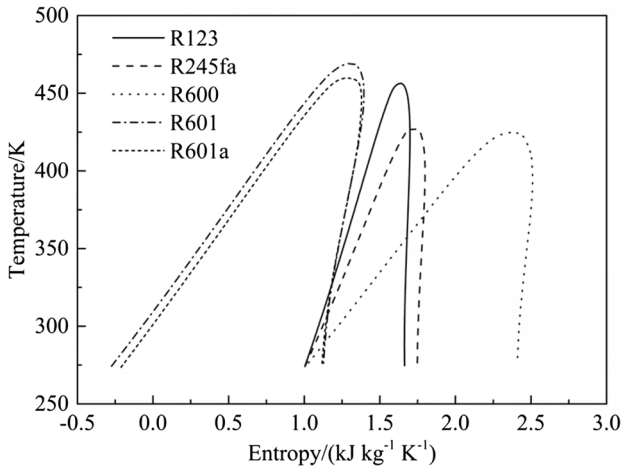

Fig. 1 Temperature–entropy diagram of five types of working fluids

Table 1 Characteristic parameters of five types of working fluids

Working fluids	R123	R245fa	R600	R601	R601a
Type	HCFC	HFC	HC	HC	HC
Molar mass/(g mol^{-1})	152.930	134.050	58.122	72.150	72.150
Boiling point/°C	27.82	14.90	−0.49	36.06	27.83
Critical temperature/°C	183.68	154.05	152.00	196.55	187.20
Critical pressure/MPa	3.662	3.651	3.796	3.371	3.378
ODP	0.02	0	0	0	0
GWP	93	950	20	11	7

3 Thermodynamic analysis of ORC system

The structure schematic diagram of an ORC system for waste heat recovery of sinter cooling flue gas is shown in Fig. 2a. The cooling flue gas expelled from the end of the sinter annular cooler is firstly sent into the evaporator of the thermal system and then discharged from the flue gas outlet of the evaporator after heat exchange with the working fluid in the evaporator. The working fluid in the evaporator is heated into saturated or overheated vapor and then expands to do work in the expander. The vapor exhaust of working fluid discharged from the outlet of the expander is condensed into the saturated fluid in the condenser, and the saturated fluid is sent into the evaporator for reuse through the pump.

When the cycle process of the thermal system is in a stable state and the system has no heat dissipation, as known from the T–s diagram of the ORC system shown in Fig. 2b, the process (2-3) is the adiabatic expansion process, and the working fluid expands to do work in the expander. The process (3–5) is the isobaric condensation process, and the working fluid is condensed into the saturated fluid in the condenser. The process (5–6) is the adiabatic compression process, and the working fluid is pressurized by the pump. The process (6–2) is the isobaric heating process, and the working fluid is heated into saturated or overheated vapor in the evaporator. When the working fluid at the outlet of the evaporator is the saturated vapor, the state point 1 is coincident with the state point 2.

Based on the first and second laws of thermodynamics, and combined with the T–s diagram of the ORC system shown in Fig. 2b, the thermodynamic process of the ORC system is described as follows.

In the isobaric heating process (6–2), the working fluid is heated at constant pressure in the evaporator. The heat transfer capacity from the cooling flue gas to the working fluid is calculated as

$$Q_{\mathrm{ev}} = m_{\mathrm{f}}\left(h_2 - h_6\right) \tag{1}$$

where Q_{ev} is the heat transfer capacity in the evaporator; m_{f} is the mass flow rate of working fluid; h_2 is the enthalpy of

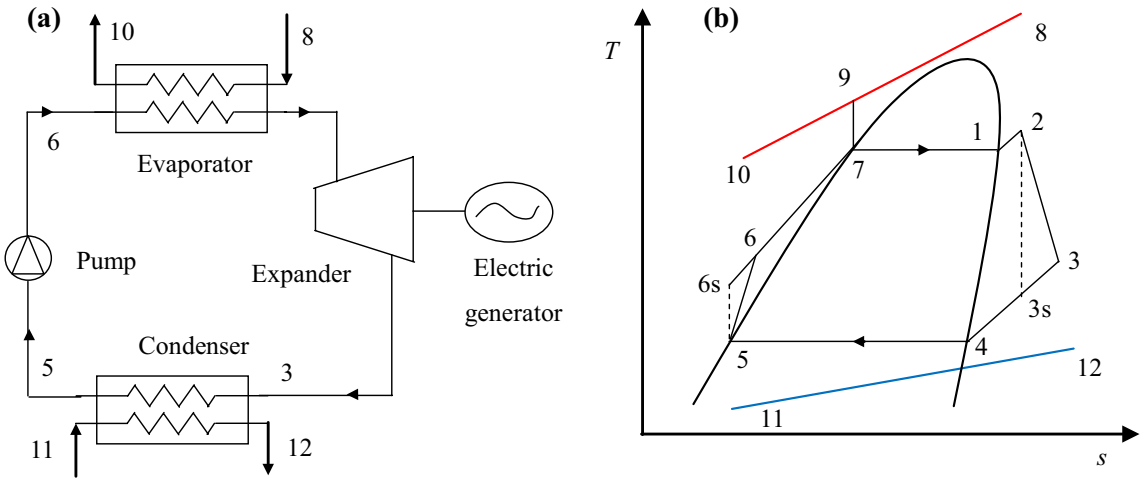

Fig. 2 Structure (**a**) and *T*–*s* (**b**) diagrams of ORC system

working fluid at the outlet of the evaporator; and h_6 is the enthalpy of working fluid at the inlet of the evaporator.

The irreversible loss generated in the endothermic process is

$$I_{ev} = m_f T_0 \left(s_2 - s_6 - \frac{h_2 - h_6}{T_s} \right) \tag{2}$$

where I_{ev} is the irreversible loss in the evaporator; T_0 is the atmospheric temperature; s_2 is the entropy of working fluid at the outlet of the evaporator; s_6 is the entropy of working fluid at the inlet of the evaporator; and T_s is the average value of inlet and outlet temperature of cooling flue gas.

In the adiabatic expansion process (2–3), the expander converts heat into work. Considering the isentropic efficiency of the expander, the actual output power of the expander is obtained as follows:

$$W_{ex} = m_f (h_2 - h_{3s}) \eta_{ex} \tag{3}$$

where W_{ex} is the power produced by the expander; h_{3s} is the ideal enthalpy of working fluid at the outlet of the expander; and η_{ex} is the isentropic efficiency of the expander, which is given as

$$\eta_{ex} = \frac{h_2 - h_3}{h_2 - h_{3s}} \tag{4}$$

where h_3 is the enthalpy of working fluid at the outlet of the expander.

The irreversible loss generated in the expansion process is

$$I_{ex} = m_f T_0 (s_3 - s_2) \tag{5}$$

where I_{ex} is the irreversible loss in the expander and s_3 is the entropy of working fluid at the outlet of the expander.

In the isobaric condensation process (3–5), the working fluid is condensed at constant pressure in the condenser. The heat transfer capacity from the working fluid to the cooling water is calculated as

$$Q_c = m_f (h_3 - h_5) \tag{6}$$

where Q_c is the heat transfer capacity in the condenser and h_5 is the enthalpy of working fluid at the outlet of condenser.

The irreversible loss generated in the condenser is

$$I_c = m_f T_0 \left(s_5 - s_3 - \frac{h_5 - h_3}{T_c} \right) \tag{7}$$

where I_c is the irreversible loss in the condenser; s_5 is the entropy of working fluid at the outlet of the condenser; and T_c is the average value of inlet and outlet temperature of cooling water.

In the adiabatic compression process (5–6), the pump converts electric power into work. Considering the isentropic efficiency of pump, the actual power consumption of the pump is obtained.

$$W_p = m_f (h_{6s} - h_5) / \eta_p \tag{8}$$

where W_p is the power required by the pump; h_{6s} is the ideal enthalpy of working fluid at the outlet of pump; and η_p is the isentropic efficiency of pump, which is given as

$$\eta_p = \frac{h_{6s} - h_5}{h_6 - h_5} \tag{9}$$

The irreversible loss generated in the compression process is

$$I_p = m_f T_0 (s_6 - s_5) \tag{10}$$

where I_p is the irreversible loss in the pump.

According to the first law of thermodynamics, the thermal efficiency of the ORC system is defined as

$$\eta_t = \frac{W}{Q_{ev}} = \frac{W_{ex} - W_p}{Q_{ev}} = \frac{(h_2 - h_3) - (h_6 - h_5)}{h_2 - h_6} \tag{11}$$

where η_t is the thermal efficiency of the ORC system; and W is the net output power of the ORC system.

The total irreversible loss of the ORC system (I_{total}) is calculated as follows.

$$I_{total} = I_{ev} + I_{ex} + I_c + I_p = m_f T_0 \left(\frac{h_6 - h_2}{T_s} - \frac{h_5 - h_3}{T_c} \right) \tag{12}$$

The exergy efficiency of the ORC system is calculated on the basis of the irreversible loss in different processes of the ORC system. The exergy efficiency is defined as the ratio of net output power to maximum work obtained by the ORC system and is given by

$$\eta_e = \frac{W}{W + I_{total}} = \frac{(h_2 - h_3) - (h_6 - h_5)}{(h_2 - h_3) - (h_6 - h_5) + T_0 \left(\frac{h_6 - h_2}{T_s} - \frac{h_5 - h_3}{T_c} \right)} \tag{13}$$

4 Results and discussion

The heat source of the ORC system in the present work is the sinter cooling flue gas at the end of a sinter annular cooler, of which the flow rate and average inlet temperature are 273 kg/s and 170 °C, respectively [28]. The thermal process of the ORC system is calculated through the combination of MATLAB and REFPROP, and the effects of evaporation temperature (T_1) and superheat degree ($\Delta T_{1-2} = T_2 - T_1$) of working fluid, as well as the pinch point temperature difference ($\Delta T_{7-9} = T_9 - T_7$) in the evaporator on the thermal performance of the ORC system, are investigated. The initial operational parameters of the ORC system are shown in Table 2 [29].

4.1 Effect of evaporation temperature of working fluid

When the pinch point temperature difference in the evaporator is 10 °C and the working fluid at the outlet of the evaporator is the saturated vapor, the variation of system net output power with the evaporation temperature of working fluid is shown in Fig. 3. As can be seen from Fig. 3, the system net output power first increases and then decreases with the increase in evaporation temperature. When the evaporation temperature is 100 °C, the system net output powers for R123, R245fa, R601 and R601a are all the maximum, while the evaporation temperature of R600 corresponding to the maximum system net output power is 110 °C. This may be explained that, with the increase in evaporation temperature, the system net output power per unit flow rate of working fluid gradually increases, but based on the first law of thermodynamics, the flow rate of working fluid gradually decreases when the flow rate and inlet temperature of sinter cooling flue gas are constant. When the evaporation temperature of working fluid is less than the temperature corresponding to the maximum system net output power, the increase amplitude of net output power per unit flow rate of working fluid is greater than the decrease amplitude of flow rate of working fluid with the increase in evaporation temperature, which results in the increase in system net output power, and vice versa.

Figure 3 also shows that the system net output power of R601 is the minimum, and it is closely followed by R123 and R601a. When the evaporation temperature of working fluid is greater than 110 °C, the net output power of R600, followed by R245fa, is the maximum among five types of working fluids. When the evaporation temperature is 100 °C

Table 2 Initial operational parameters of ORC system

Parameter	Value
Flow rate of cooling flue gas/(kg s^{-1})	273
Inlet temperature of cooling flue gas/°C	170
Inlet temperature of cooling water/°C	20
Isentropic efficiency of pump	0.8
Isentropic efficiency of expander	0.85
Condensation temperature/°C	30
Pinch point temperature difference of condenser/°C	5
Ambient temperature/°C	20

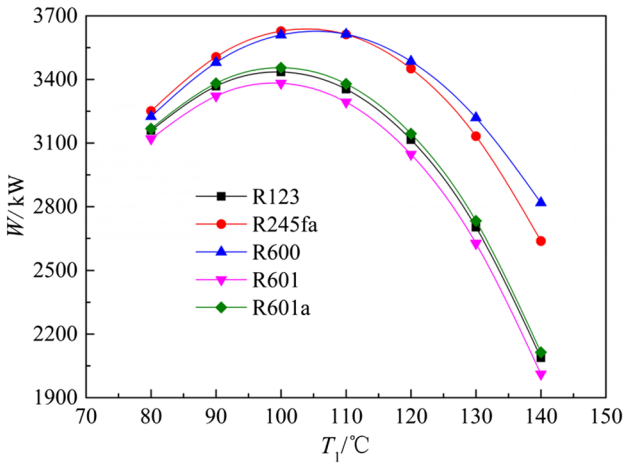

Fig. 3 Effect of evaporation temperature on system net output power

and the working fluid is R245fa, the ORC system obtains the maximum net output power of 3628 kW among five types of working fluids.

Figure 4 shows the variation of thermal efficiency of the ORC system with the evaporation temperature of working fluid. As can be seen from Fig. 4, the system thermal efficiency gradually increases with the increase in evaporation temperature for different working fluids. This may be because the change of system thermal efficiency has nothing to do with the flow rate of working fluid, and the increase in evaporation temperature also causes the increase in net output power and heat transfer capacity per unit flow rate of working fluid. Meanwhile, the increase amplitude of net output power per unit flow rate of working fluid is greater than that of heat transfer capacity per unit flow rate of working fluid, which leads to the increase in system thermal efficiency. In addition, for a given evaporation temperature, the system thermal efficiency of R123 is the maximum, and it is closely followed by R601, R601a and R600, while the system thermal efficiency of R245fa is the minimum. When the evaporation temperature of working fluid is 130 °C, the system thermal efficiencies of R123 and R245fa are 16.39% and 14.87%, respectively.

Figure 5 shows the variation of total irreversible loss of the ORC system with the evaporation temperature of working fluid. As can be seen from Fig. 5, the system total irreversible loss gradually decreases with the increase in evaporation temperature for different working fluids. This may be because the increase in evaporation temperature results in the decrease in flow rate of working fluid according to the first law of thermodynamics. Meanwhile, the increase in evaporation temperature also leads to the decrease in heat transfer temperature difference between the cooling flue gas and working fluid in the evaporator, which results in the decrease in irreversible loss in the evaporator and the system total irreversible loss.

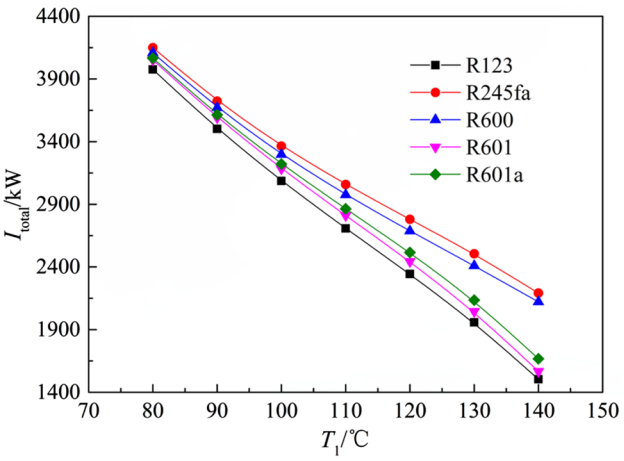

Fig. 5 Effect of evaporation temperature on system total irreversible loss

Figure 5 also shows that for a given evaporation temperature, the system total irreversible loss of R123 is the minimum, and it is closely followed by R601, R601a and R600, while the system total irreversible loss of R245fa is the maximum. In addition, the downtrend of system total irreversible loss of R245fa is slower than that of R123 and basically the same with that of R600, while the downtrend of system total irreversible loss of R123 is basically the same with that of R601 and R601a. When the evaporation temperature of working fluid increases by 10 °C, the average total irreversible loss of R245fa decreases by 326.5 kW, while the average total irreversible loss of R123 decreases by 412 kW.

Figure 6 shows the variation of exergy efficiency of the ORC system with the evaporation temperature of working fluid. As can be seen from Fig. 6, the system exergy

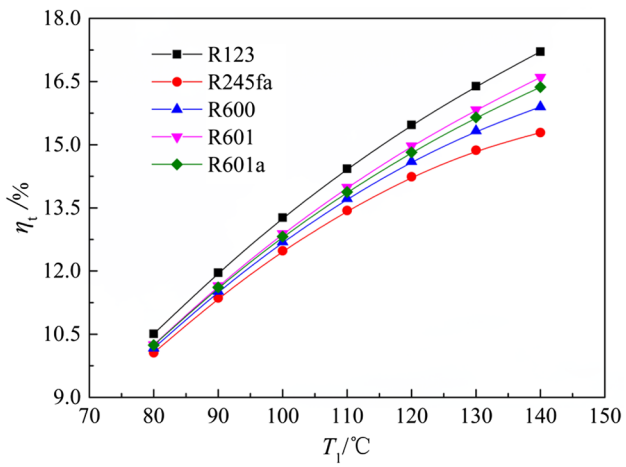

Fig. 4 Effect of evaporation temperature on system thermal efficiency

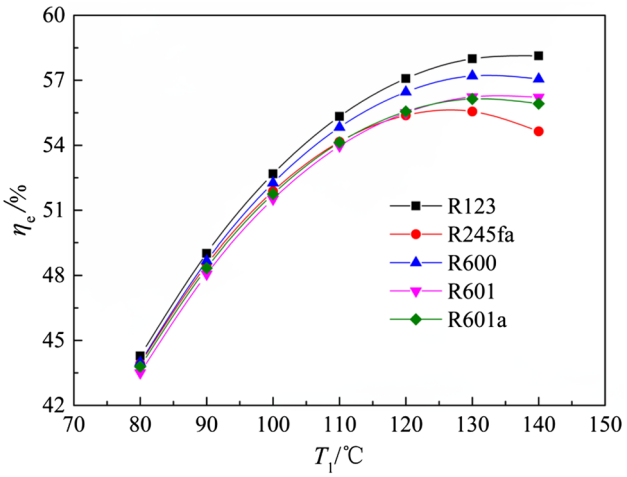

Fig. 6 Effect of evaporation temperature on system exergy efficiency

efficiency gradually increases with the increase in evaporation temperature when the evaporation temperature is less than 130 °C. When the evaporation temperature is greater than 130 °C, with the increase in evaporation temperature, the system exergy efficiencies of R245fa, R601, R601a and R600 gradually decrease, which means that the ORC system with the evaporation temperature of 130 °C for R245fa, R601, R601a and R600 could obtain the maximum exergy efficiency, while the system exergy efficiency of R123 continues to increase, but the increase amplitude of exergy efficiency is very small. Through the theoretical calculation of evaporation temperature ranges (130–140 °C) for the working fluid of R123, when the evaporation temperature is 136 °C, the ORC system with the working fluid of R123 obtains the maximum exergy efficiency, namely 58.17%. When the evaporation temperature is greater than 136 °C, the system exergy efficiency of R123 gradually decreases with the increase in evaporation temperature. In addition, the system exergy efficiency of R123 is the maximum among five types of working fluids. When the evaporation temperature is 130 °C, the system exergy efficiency of R123 is 57.99%, while the system exergy efficiency of R245fa is 55.56%, which is the minimum among five types of working fluids.

4.2 Effect of superheat degree of working fluid

When the pinch point temperature difference in the evaporator is 10 °C and the evaporation temperature of working fluid is 130 °C, the variation of system net output power with the superheat degree of working fluid is shown in Fig. 7. As can be seen from Fig. 7, the system net output power gradually decreases with the increase in superheat degree. This may be explained that the increase in superheat degree of working fluid causes the increase in net output power per unit flow rate of working fluid. Meanwhile, the increase in superheat degree also results in the decrease in heat transfer temperature difference between the cooling flue gas and working fluid in the evaporator, which leads to the decrease in flow rate of working fluid according to the first law of thermodynamics. Because the decrease amplitude of flow rate of working fluid is greater than the increase amplitude of net output power per unit flow rate of working fluid, the system net output power gradually decreases with the increase in superheat degree.

Figure 7 also shows that for a given superheat degree, the system net output power of R600 is the maximum, while the system net output power of R601 is the minimum. When the superheat degree of working fluid is greater than 5 °C, the system net output power of R123 is larger than that of R601a, and vice versa. In addition, the decrease amplitude of system net output power of R600 is greater than that of R601 with the increase in superheat degree. When the superheat degree of working fluid increases by 2 °C, the average net output power of R600 decreases by 50.7 kW, while the average net output power of R601 decreases by 25.3 kW.

Figure 8 shows the variation of thermal efficiency of the ORC system with the superheat degree of working fluid. As can be seen from Fig. 8, with the increase in superheat degree, the system thermal efficiencies of R123, R245fa and R600 gradually increase, while the system thermal efficiencies of R601 and R601a gradually decrease. This may be explained that the increase in superheat degree results in the increase in net output power and heat transfer capacity per unit flow rate of working fluid. For the working fluids of R123, R245fa and R600, the increase amplitude of net output power per unit flow rate of working fluid is greater than that of heat transfer capacity per unit flow rate of working fluid, while for the working fluids of R601 and R601a, the heat transfer capacity per unit flow rate of working fluid is

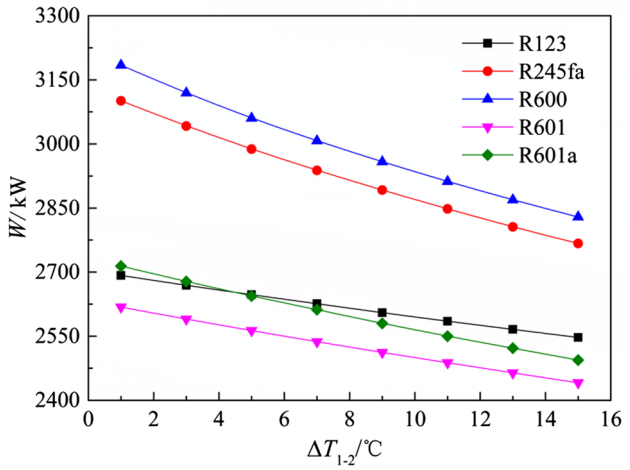

Fig. 7 Effect of superheat degree on system net output power

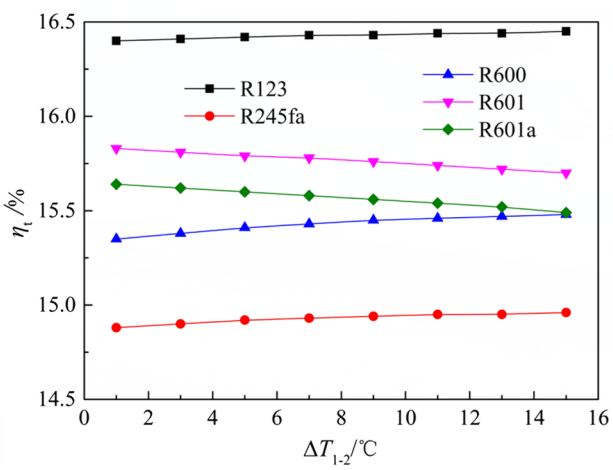

Fig. 8 Effect of superheat degree on system thermal efficiency

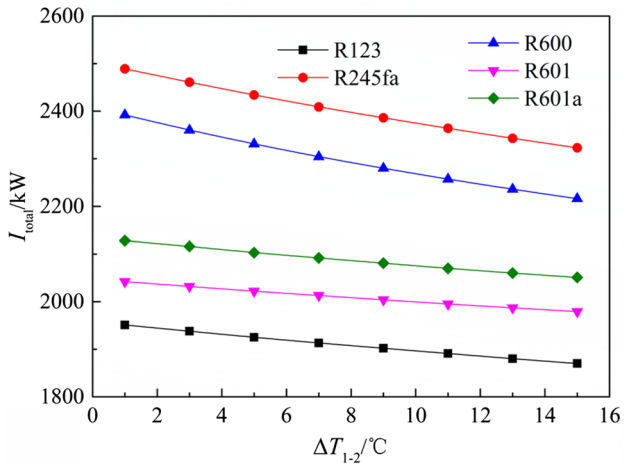

Fig. 9 Effect of superheat degree on system total irreversible loss

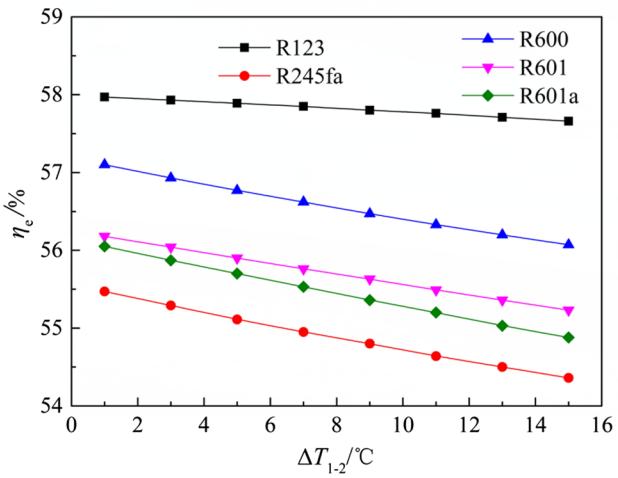

Fig. 10 Effect of superheat degree on system exergy efficiency

relatively larger. In addition, for a given superheat degree, the system thermal efficiency of R123 is the maximum, and the system thermal efficiency of R245fa is the minimum. When the superheat degree of working fluid is greater than 15 °C, the system thermal efficiencies of R600 will be greater than those of R601a.

Figure 9 shows the variation of total irreversible loss of the ORC system with the superheat degree of working fluid. As can be seen from Fig. 9, the system total irreversible loss all gradually decreases with the increase in superheat degree for five types of working fluids. This may be because the increase in superheat degree also leads to the decrease in flow rate of working fluid. Meanwhile, the increase in superheat degree causes the decrease in heat transfer temperature difference between the cooling flue gas and working fluid in the evaporator, which leads to the decrease in irreversible loss in the evaporator and the system total irreversible loss.

Figure 9 also shows that for a given superheat degree, the system total irreversible loss of R123 is the minimum, and the system total irreversible loss of R245fa is the maximum. In addition, the downtrend of system total irreversible loss of R245fa is faster than that of R123 with the increase in superheat degree. When the superheat degree of working fluid increases by 2 °C, the average total irreversible loss of R245fa decreases by 23.7 kW, while the average total irreversible loss of R123 decreases by 11.6 kW.

Figure 10 shows the variation of exergy efficiency of the ORC system with the superheat degree of working fluid. As can be seen from Fig. 10, the system exergy efficiency of different working fluids gradually decreases with the increase in superheat degree. The reason is that the increase in superheat degree results in the decrease in system net output power and total irreversible loss at the same time. According to the calculation results shown in Figs. 7 and 9, the decrease amplitude of system net output power is larger than that of system total irreversible loss, which leads to the decrease in system exergy efficiency.

Figure 10 also shows that for a given superheat degree, the system exergy efficiency of R123 is the maximum, and the system exergy efficiency of R245fa is the minimum. Meanwhile, the downtrend of system exergy efficiency of R123 is slower than that of R245fa with the increase in superheat degree. When the superheat degree of working fluid increases by 2 °C, the system exergy efficiency of R123 decreases by 0.044%, while the average system exergy efficiency of R245fa decreases by 0.159%.

4.3 Effect of pinch point temperature difference in evaporator

When the evaporation temperature of working fluid is 130 °C and the working fluid at the outlet of the evaporator is the saturated vapor, the variation of system net output power with the pinch point temperature difference in the evaporator is shown in Fig. 11. As can be seen from Fig. 11, the system net output power of different working fluids gradually decreases with the increase in pinch point temperature difference. The reason may be that, as known from Fig. 2b, the increase in pinch point temperature difference results in the increase in outlet temperature of cooling flue gas in the evaporator, which leads to the decrease in flow rate of working fluid according to the first law of thermodynamics. Because the system net output power per unit flow rate of working fluid is constant, the system net output power gradually decreases.

Figure 11 also shows that for a given pinch point temperature difference, the system net output power of R600 is the maximum, and it is closely followed by R245fa, R601a and R123, while the system net output power of R601 is the minimum. In addition, the downtrend of system net output

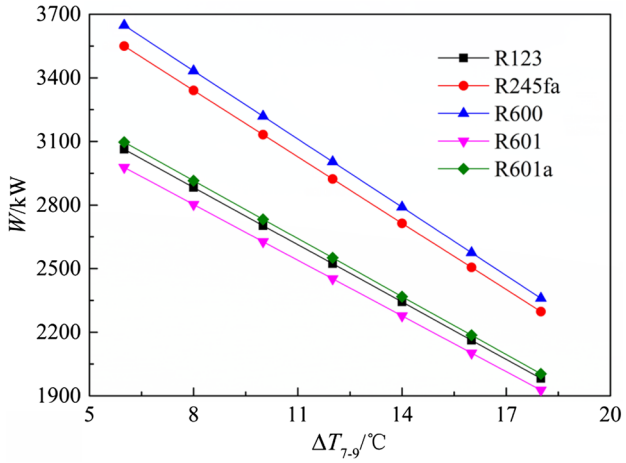

Fig. 11 Effect of pinch point temperature difference on system net output power

power of R600 is faster than that of R601 and basically the same with that of R245fa with the increase in pinch point temperature difference. When the pinch point temperature difference increases by 2 °C, the average net output power of R600 decreases by 214.7 kW, while the average net output power of R601 decreases by 175.2 kW.

Figure 12 shows the variation of thermal efficiency of the ORC system with the pinch point temperature difference. As can be seen from Fig. 12, the system thermal efficiencies for five types of working fluids are constant with the increase in pinch point temperature difference. This may be because the evaporation temperature and condensation temperature are constant, and the system net output power and heat transfer capacity per unit flow rate of working fluid are also constant. Meanwhile, the change in flow rate of working fluid has no effect on the system thermal efficiency, which results in the constant system thermal efficiency. For different pinch point temperature differences, the system thermal efficiencies of R123 and R245fa are 16.39% and 14.87%, which are the maximum and minimum thermal efficiencies, respectively.

Figure 13 shows the variation of total irreversible loss of the ORC system with the pinch point temperature difference. As can be seen from Fig. 13, the system total irreversible loss gradually decreases with the increase in superheat degree for different working fluids. The reason may be that the increase in pinch point temperature difference results in the decrease in flow rate of working fluid, and the average value of inlet and outlet temperature of cooling flue gas also gradually increases, which leads to the decrease in irreversible loss in the evaporator and the system total irreversible loss.

Figure 13 also indicates that with the increase in pinch point temperature difference, the downtrend of system total irreversible losses for five types of working fluids is basically the same, and the system total irreversible losses of R245fa and R123 are the maximum and minimum, respectively. When the pinch point temperature difference of working fluid increases by 2 °C, the average total irreversible loss decreases by 83.6 kW.

Figure 14 shows the variation of exergy efficiency of the ORC system with the pinch point temperature difference. As can be seen from Fig. 14, the system exergy efficiency of different working fluids gradually decreases with the increase in pinch point temperature difference. This may be due to the decrease in system net output power and total irreversible loss at the same time caused by the increase in pinch point temperature difference, and the decrease amplitude of system net output power is larger than that of system total irreversible loss according to the calculation results shown

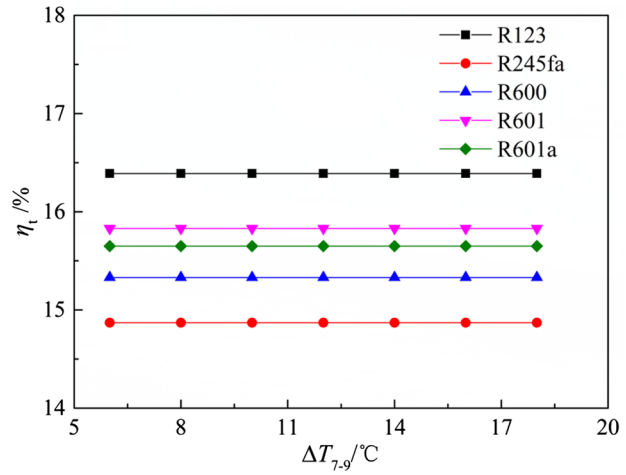

Fig. 12 Effect of pinch point temperature difference on system thermal efficiency

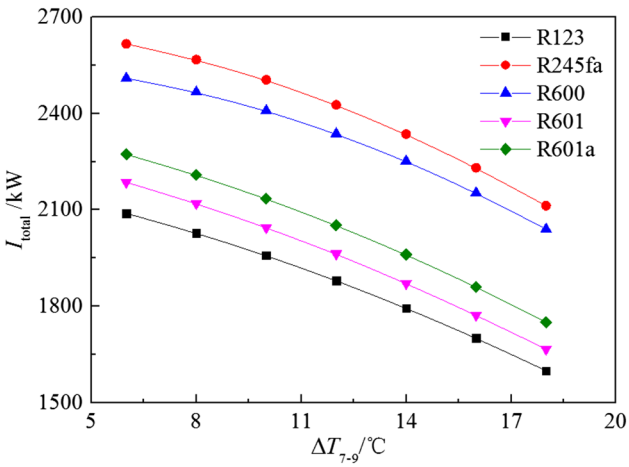

Fig. 13 Effect of pinch point temperature difference on system total irreversible loss

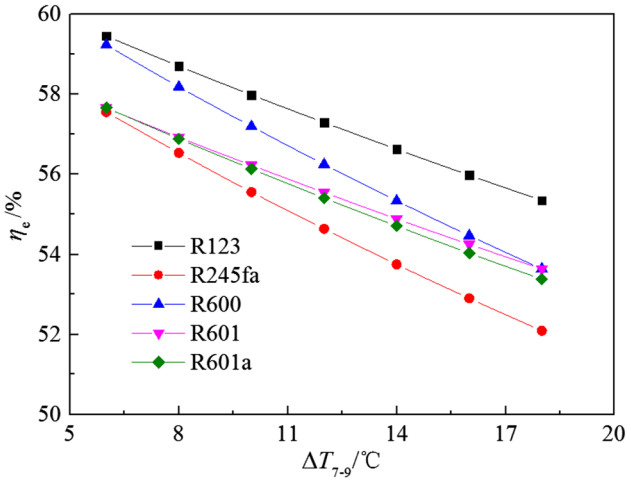

Fig. 14 Effect of pinch point temperature difference on system exergy efficiency

in Figs. 11 and 13, which leads to the decrease in system exergy efficiency.

Figure 14 also shows that when the pinch point temperature difference is greater than 6 °C, the system exergy efficiency of R123 is the maximum, and that of R245fa is the minimum with the increase in pinch point temperature difference. In addition, the downtrend of system exergy efficiency of R245fa is faster than that of R123 and basically the same with that of R600. When the pinch point temperature difference in the evaporator increases by 2 °C, the system exergy efficiency of R123 decreases by 0.685%, while the average system exergy efficiencies of R245fa and R600 decrease by 0.922%.

5 Conclusions

1. The system net output power first increases and then decreases with the increase in evaporation temperature and decreases with the increase in superheat degree and pinch point temperature difference. The system net output power of R601 is the minimum, and the net output power of R600 is the maximum when the evaporation temperature is greater than 110 °C. The effect of pinch point temperature difference on the system net output power is larger than that of superheat degree, and the ORC system could obtain the maximum net output work through the adjustment of evaporation temperature of working fluid.
2. The system thermal efficiencies of R123, R245fa and R600 gradually increase with the increase in evaporation temperature and superheat degree, and the system thermal efficiencies of R601 and R601a gradually increase with the increase in the evaporation temperature and decrease in the superheat degree. The change in pinch point temperature difference has no effect on the system thermal efficiency. For a given operational condition, the system thermal efficiency of R123 is the maximum, while the system thermal efficiency of R245fa is the minimum.
3. The system total irreversible loss gradually decreases with the increase in the evaporation temperature, superheat degree and pinch point temperature difference. The system total irreversible loss of R123 is the minimum, while the system total irreversible loss of R245fa is the maximum. The effect of pinch point temperature difference on the system total irreversible loss is larger than that of evaporation temperature and superheat degree.
4. The system exergy efficiency also first increases and then decreases with the increase in evaporation temperature and decreases with the increase in superheat degree and pinch point temperature difference. The system exergy efficiency of R123 is the maximum among five types of working fluids, and the system exergy efficiency of R245fa is the minimum when the evaporation temperature is greater than 120 °C. The ORC system could also obtain the maximum exergy efficiency through the adjustment of evaporation temperature of working fluid.
5. Because the change in superheat degree has little effect on the system thermal efficiency, the status of working fluid at the outlet of the evaporator should be set as the saturated vapor in the practical operation to obtain the maximum system net output power and exergy efficiency. Meanwhile, the type and evaporation temperature of working fluid are also selected reasonably, as well as the pinch point temperature difference in the evaporator.

Acknowledgements We would like to acknowledge financial support for this work provided by the National Natural Science Foundation of China (5171101721, 51974087), China Postdoctoral Science Foundation (2018M642538), Fundamental Research Funds for the Central Universities (WK2090130025) and Anhui Provincial Natural Science Foundation (1908085QE203).

References

[1] J.J. Cai, J.J. Wang, C.X. Chen, Z.W. Lu, Iron and Steel 42 (2007) No. 6, 1–7.
[2] L.G. Chen, H.J. Feng, Z.H. Xie, Entropy 18 (2016) 353.
[3] X. Shen, L.G. Chen, S.J. Xia, Z.H. Xie, X.Y. Qin, J. Clean. Prod. 172 (2018) 2153–2166.
[4] H. Dong, H.Y. Lin, H.H. Zhang, J.J. Cai, C.B. Xu, J.W. Zhou, Iron and Steel 46 (2011) No. 11, 93–98.
[5] H. Dong, Y. Zhao, J.J. Cai, J.W. Zhou, G.Y. Ma, Iron and Steel 47 (2012) No. 1, 95–99.
[6] H. Chen, D.Y. Goswami, E.K. Stefanakos, Renew. Sust. Energ. Rev. 14 (2010) 3059–3067.

[7] Z.H. Han, Y. Du, Z. Wang, Chemical Industry and Engineering Progress 33 (2014) 2279–2285.
[8] D.X. Li, S.S. Zhang, G.H. Wang, J. Hydrodyn. 27 (2015) 458–464.
[9] E.H. Wang, H.G. Zhang, B.Y. Fan, M.G. Ouyang, Y. Zhao, Q.H. Mu, Energy 36 (2011) 3406–3418.
[10] R. Long, Y.J. Bao, X.M. Huang, W. Liu, Energy 73 (2014) 475–483.
[11] E. Saloux, M. Sorin, H. Nesreddine, A. Teyssedou, Appl. Therm. Eng. 129 (2018) 628–635.
[12] Ö. Kaşka, Energ. Convers. Manage. 77 (2014) 108–117.
[13] A. Javanshir, N. Sarunac, Z. Razzaghpanah, Appl. Therm. Eng. 123 (2017) 852–864.
[14] F.B. Xie, T. Zhu, N.P. Gao, CIESC J. 67 (2016) 4111–4117.
[15] M.Q. Fan, T. Zhou, Z.Q. Sun, J.M. Zhou, Journal of Central South University (Science and Technology) 47 (2016) 1030–1038.
[16] K.C. Pang, S.C. Chen, T.C. Hung, Y.Q. Feng, S.C. Yang, K.Y. Wong, J.R. Lin, Energy 133 (2017) 636–651.
[17] L. Li, Y.T. Ge, X. Luo, S.A. Tassou, Appl. Therm. Eng. 115 (2017) 815–824.
[18] J.P. Roy, M.K. Mishra, A. Misra, Energy 35 (2010) 5049–5062.
[19] J.P. Roy, A. Misra, Energy 39 (2012) 227–235.
[20] S. Cignitti, J.G. Andreasen, F. Haglind, J.M. Woodley, J. Abildskov, Appl. Energ. 203 (2017) 442–453.
[21] C.J.N. Sanchez, L. Gosselin, A.K. da Silva, Energ. Convers. Manage. 156 (2018) 585–596.
[22] W.J. Chen, H.J. Feng, L.G. Chen, S.J. Xia, J. Therm. Sci. 27 (2018) 555–562.
[23] Y.C. Shao, H. Dong, Y.J. Sun, F.W. Wang, C.T. Chen, Sintering and Pelletizing 39 (2014) No. 4, 50–54.
[24] Z.L. Chen, X.C. Cao, Energy for Metallurgical Industry 36 (2017) No. 1, 41–44.
[25] O. Badr, S.D. Probert, P.W. O'callaghan, Appl. Energ. 21 (1985) 1–42.
[26] V. Maizza, A. Maizza, Appl. Therm. Eng. 16 (1996) 579–590.
[27] G. Angelino, P.C. di Paliano, Energy 23 (1998) 449–463.
[28] J.S. Feng, H. Dong, A.H. Wang, Q. Zhang, J.J. Cai, J. Iron Steel Res. 27 (2015) No. 6, 7–11.
[29] Z.H. Han, Y.L. Ye, Y. Liu, Journal of Chinese Society of Power Engineering 32 (2012) 229–234.